SLAC-PUB-15469

Demonstration of Cascaded Optical Inverse Free-Electron Laser Accelerator

M. Dunning, E. Hemsing, C. Hast, T.O. Raubenheimer, S. Weathersby and D. Xiang*
SLAC National Accelerator Laboratory, Menlo Park, CA, 94025, USA

F. Fu†
Department of Physics, Shanghai Jiao Tong University, Shanghai, 200240, China
(Dated: May 21, 2013)

We report on a proof-of-principle demonstration of a two-stage cascaded optical inverse free-electron laser (IFEL) accelerator in which an electron beam is accelerated by a strong laser pulse after being packed into optical micro-bunches by a weaker initial laser pulse. We show experimentally that injection of precisely prepared optical micro-bunches into an IFEL allows net acceleration or deceleration of the beam, depending on the relative phase of the two laser pulses. The experimental results are in excellent agreement with simulation. The demonstrated technique holds great promise to significantly improve the beam quality of IFELs and may have a strong impact on emerging laser accelerators driven by high-power optical lasers.

PACS numbers: 41.75.Jv, 41.60.Cr, 41.75.Ht

Particle accelerators have played a key role in the development of physics, chemistry, biology, and material science. For instance, in particle physics, elementary particles are accelerated to high energy and then collided with other particles for studying fundamental laws of nature (see, for example [1]). In accelerator-based photon science, the high energy electron beams are used to produce intense x-rays (see, for example [2]) that researchers use to probe molecules, atoms, crystals, and innovative new materials in order to better understand their structure and behavior. Limited by the gradient limits (∼100 MeV/m) in microwave accelerating structures, high-energy beams require massive and costly machines.

To reduce the size and cost of these scientific facilities, various laser-based advanced acceleration techniques such as the laser wake-field accelerator (LWFA) [3–5] and inverse free-electron laser (IFEL) [6–10] have been proposed and demonstrated to provide much higher accelerating gradients. While the LWFAs driven by high-power optical lasers (e.g. Ti:Sapphire laser with wavelength around 800 nm) have been extensively studied (see, for example [11]), optical IFELs have remained largely undeveloped due in large part to the fact that the synchrotron radiation losses, together with the energy dependent acceleration rate, make it difficult to use IFELs for accelerating beams to TeV energies. However, the recent discovery of the Higgs-like boson at LHC [12, 13] in the more accessible 125 GeV range has renewed interest in the development of a compact electron-positron collider based on the IFEL. Furthermore, IFELs may be particularly suited for compact gamma ray sources based on inverse Compton scattering (ICS), because the high-power lasers can be used for both the electron acceleration and the ICS interaction [14–16].

In an IFEL [6] the electrons interact resonantly with a collinear high-power laser in an undulator, wherein the alternating magnetic field makes the electrons wiggle in the transverse direction. For a planar undulator, sustained energy exchange between the electrons and the laser is achieved when the resonant condition is met, i.e. $\lambda = (1+K^2/2)\lambda_u/2n\gamma^2$, where λ is the laser wavelength, λ_u the undulator period, K the dimensionless undulator strength, $n = 1, 3, 5, 7, \ldots$ an odd number and γ the relativistic energy of the beam. At the exit of the undulator, an electron's energy changes by $\delta E = \int \vec{v_e} \cdot \vec{E_l}$, where $\vec{v_e}$ is the transverse velocity of the electron and $\vec{E_l}$ is the field of the laser.

In general the electron bunch length is much longer than the laser wavelength. Therefore, depending on the relative position of an electron in the laser field of a single stage IFEL, some of the electrons will be accelerated

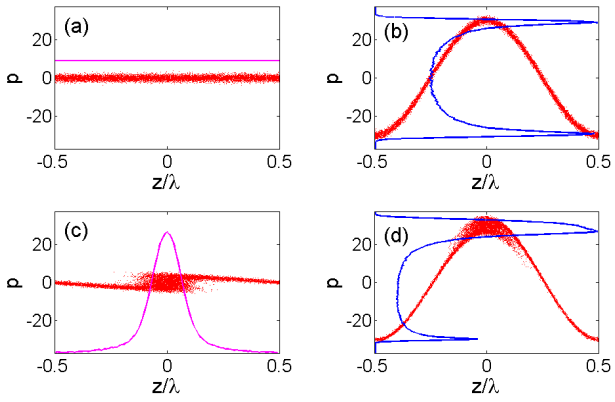

FIG. 1: Initial and final beam longitudinal phase space in an IFEL for an unmodulated beam [(a) and (b)] and a pre-bunched beam [(c) and (d)]. The corresponding beam current and energy distributions are illustrated with magenta and blue lines, respectively. The horizontal axis is the beam longitudinal position normalized to the laser wavelength and the vertical axis is particle's energy deviation with respect to the reference particle normalized to the rms slice energy spread of the beam. The maximal energy change is assumed to be 30 times larger than the beam energy spread.

Work supported in part by US Department of Energy under contract DE-AC02-76SF00515.

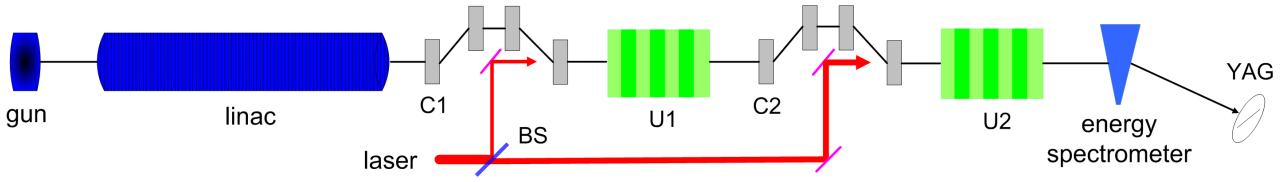

FIG. 2: Schematic layout of the cascaded optical IFEL accelerator experiment at SLAC's NLCTA.

while the rest will be decelerated. To reach high energies more efficiently, the undulator is typically tapered such that its period and magnetic field vary in the longitudinal direction to follow the energy change of the accelerated particles. In this case the resonant condition for the accelerated particles is always met, allowing them to have continuous and effective energy exchange with the laser. However, the rest of the particles, which are outside the accelerating bucket, fall out of resonance and their energy remains essentially unchanged. Based on this 'self-trapping' mechanism, a single stage IFEL is characterized by limited trapping efficiency and relatively large beam energy spread [10, 17].

Injection of micro-bunches in IFELs, in which the electrons are piled up at the laser wavelength to match the periodic accelerating buckets of the optical laser field, would greatly increase the trapping efficiency and reduce the final beam energy spread. The advantage of this cascaded method is illustrated in Fig. 1 where we assume the bandwidth of the undulator is larger than the beam energy spread. In a single stage IFEL, it can be clearly seen that when electrons with randomly distributed phases are injected (Fig. 1a), half of the electrons are accelerated while the other half are decelerated (Fig. 1b). In contrast, with a pre-bunched beam (Fig. 1c), most of the beam can be accelerated and a large percentage of the particles can be boosted to approximately the same energy (Fig. 1d). This pre-bunched beam can be readily prepared using a simple modulator-chicane system [18] (the contrast of the pre-bunched beam can be enhanced with multi-color pre-bunchers [19–21] or multiple modulator-chicane systems [22]).

Injection of micro-bunches in IFEL has been demonstrated at mid-IR wavelengths (10.6 μm) with CO_2 lasers [8, 9]. Cascading at optical wavelengths has been tested in an inverse transition radiation accelerator [23], but with net energy shift on the order of 1 keV, much smaller than beam energy spread. In this Letter, we report a proof-of-principle demonstration of a cascaded IFEL at optical wavelengths (λ =800 nm), a spectral region where high-power lasers are widely available. In this experiment, the electron beam is first packed into optical micro-bunches with a low intensity laser, and injection of these precisely prepared micro-bunches into the second undulator with a high intensity laser allows net acceleration or deceleration of the beam, depending on the relative phase of the two laser pulses.

The schematic layout of the experiment carried out at SLAC's Next Linear Collider Test Accelerator (NLCTA) [24, 25] is shown in Fig. 2. The electron beam with ~20 pC charge is generated in a 1.6 cell S-band (2.856 GHz rf frequency) photocathode rf gun with a UV laser (1 ps FWHM) and further accelerated to 120 MeV with X-band (11.424 GHz rf frequency) linac structures. The main elements of the beamline consist of two chicanes (C1 and C2), two undulators (U1 and U2), and one energy bend spectrometer.

As illustrated in Fig. 2, a Ti:Sapphire laser (1 ps FWHM) with central wavelength at 800 nm is split into two pulses with a beam splitter (BS) with 25%/75% ratio. Chicane C1 is used to generate an orbit bump to allow injection of the first laser pulse (low intensity, ~80 μJ) into the first undulator U1 (10 periods with a period of 3.3 cm and a K value of 1.82) where the laser interacts with the electron beam to imprint a sinusoidal energy modulation. Chicane C2 is used to convert the energy modulation into a density modulation such that the beam is transformed to optical micro-bunches equally separated at the laser wavelength [18]. The second laser pulse (high intensity, ~250 μJ) then interacts with the optical micro-bunches in U2 (10 periods with a period of 5.5 cm and a K value of 2.76) to produce a significant net energy shift, which is directly measured with a Yttrium Aluminum Garnet (YAG) screen downstream of the energy spectrometer. It should be pointed out that U2 is resonant at 2.4 μm, so the beam energy change in U2 is from the third harmonic interaction between the electron beam and the 800 nm laser.

In this experiment, velocity bunching [26] was used to reduce the electron bunch duration to about 0.5 ps (FWHM). This minimizes the global beam energy spread (about 20 keV FWHM) after it is accelerated in the linac structure. Furthermore, by making the beam much shorter than the laser pulse, most of the particles experience approximately the same peak energy modulation amplitude, which is critical both for the generation of uniform optical micro-bunches and for the measurement of net energy change. With quadrupole magnets (not shown) upstream of the energy spectrometer set to minimize the horizontal beta function at the YAG screen (with dispersion of 1.5 m), the optimized beam energy distribution (energy deviation with respect to the average beam energy) measured at the YAG screen is shown in Fig. 3a. The distribution has a sharp edge on the right side (corresponding to the on-crest particles with the highest energy) and a short tail on the left (corresponding to the off-crest particles). From the sharp edge, the energy resolution in our measurement is estimated to

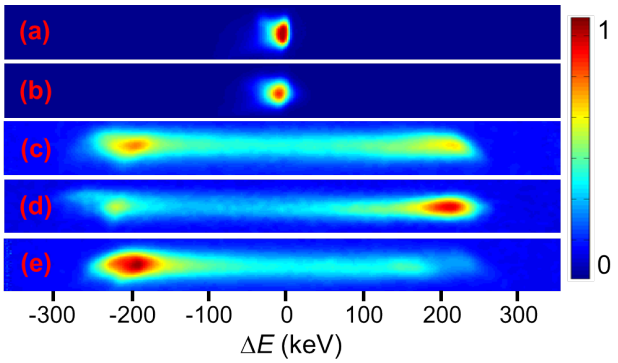

FIG. 3: Measured beam energy distribution: (a) with both lasers off; (b) with only the first laser on; (c) with only the second laser on; (d) net acceleration with both lasers on; (e) net deceleration with both lasers on. The beam intensity in (a) and (b) is reduced by a factor of 7 to avoid saturation using the same scaling as (c), (d) and (e).

be approximately 7 keV.

Following the procedures described in [24, 25], the laser pulses are made to overlap with the electron beam both in time and space. With the first laser pulse blocked, the beam energy distribution from the second laser pulse has a double-horn shape, as shown in Fig. 3c. This shape can only be obtained when the transverse electron beam size ($\sigma_e \approx 100$ μm) is smaller than the laser spot size ($\sigma_l \approx 800$ μm), and when the electron bunch length is shorter than the laser pulse length such that the modulation amplitude is roughly uniform across the whole bunch [27]. Because the electron beam is uniformly distributed across the laser bucket, half of the particles are accelerated while the other half are decelerated. This, together with the rf curvature results in a double-horn shape in beam energy distribution, with the low-energy horn slightly larger than the high-energy horn. The separation of the two horns equals approximately twice the peak energy modulation which is found to be about 200 keV, in good agreement with that obtained with an analytical formulae [28].

The first laser is then unblocked, and its intensity is finely adjusted with a polarizer to produce the optimal energy modulation (about 13 keV in this experiment with the momentum compaction of chicane C2 set to $R_{56} = 1.8$ mm) for shaping the beam into optical micro-bunches. The presence of optical micro-bunches is evident by observing the coherent emission of the undulator radiation in U2 with the second laser blocked [24, 25]. With both lasers unblocked, the resulting beam energy distribution shows large shot-to-shot fluctuations in the amplitude of the two energy horns. Depending on the relative phase of the two laser modulations imprinted on the beam, the beam is either net accelerated (Fig. 3d) or net decelerated (Fig. 3e). It can be clearly seen that, compared to the single stage IFEL case in Fig. 3c, the cascaded IFEL setup shown in Fig. 3d and Fig. 3e results in more particles experiencing approximately the net energy shift from the second laser pulse.

It should be pointed out that while the two laser pulses originate from the same source and therefore are naturally locked in phase, shot-to-shot fluctuations in beam energy result in variations in beam arrival time in U2, which modifies the relative phase of the laser modulations. Additional timing jitter between the two laser pulses could be caused by vibrations of the mirrors for laser transport as well, but this is estimated to be much smaller than the laser wavelength. In this experiment, the dominant timing jitter is from the 4×10^{-4} beam energy jitter, which translates to an rms temporal jitter of about 2.4 fs after passing through C2 (the path length in C2 is energy-dependent). With the timing jitter comparable to the laser wavelength, random fluctuations in the relative phase of the laser modulations are expected. Given this energy jitter level, locking the phase of the laser modulations would require one to reduce the R_{56} of chicane C2 by one order of magnitude, for which case the laser modulation from the first laser needs to be accordingly increased by one order of magnitude to produce optical micro-bunches. This would make the energy modulation from the first laser comparable to that from the second laser (limited by the available laser energy in our experiment), hindering clear demonstration of net energy shift in the cascaded IFEL setup. Nevertheless, in an ideal cascaded IFEL where a high power laser (>TeraWatt) would be used to significantly boost the beam energy in the second stage (for instance, a 20 TW laser may accelerate an electron beam to 1 GeV in a 1 m long undulator [17]), producing a slightly larger modulation in the first stage to reduce the beam timing jitter for phase locking is necessary and acceptable.

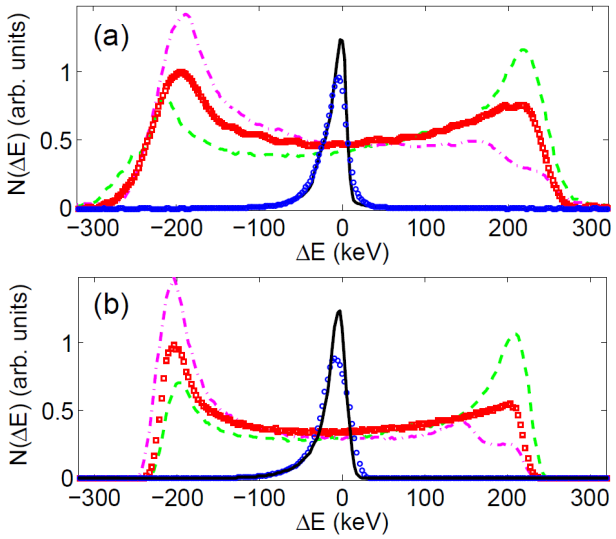

FIG. 4: Beam energy distributions in experiment (a) and simulation (b): with both lasers off (black solid lines); with only the first laser on (blue circles); with only the second laser on (red squares); net acceleration with both lasers on (green dashed lines); (e) net deceleration with both lasers on (magenta dashed-dotted lines).

For convenience of comparison, the measured energy distributions in Fig. 3 are projected in Fig. 4a where the advantage of cascading is clearly seen. The large asymmetry in beam energy distributions from the net shifted electrons (green dashed and magenta dashed-dotted lines in Fig. 4a) demonstrate the potential for improved monoenergetic beams in cascaded IFELs. The experimental results are found to be in excellent agreement with simulations (Fig. 4b) using realistic beam and laser parameters. In fact, not only are the general shapes of the experimentally measured beam distributions in the two scenarios quite similar to those obtained in simulation, the fine structures are also well reproduced. For instance, the measured beam energy distribution for the net deceleration case (magenta dashed-dotted line in Fig. 4a) has two local peaks around $\Delta E = 200$ keV. This shape is also seen in simulation (magenta dashed-dotted line in Fig. 4b).

The beam longitudinal phase space at the exit of the linac structure used in the simulation is shown in Fig. 5a. The electron bunch length (FWHM) is assumed to be 0.5 ps, and the nonlinear curvature from the varying rf phase along the bunch is taken into account. The energy modulation from the second laser is assumed to be 220 keV, following the value from analytical formula using the measured laser parameters. With only the second laser on, the longitudinal phase space is illustrated in Fig. 5b and shows the double-horn projected energy distribution (red squares in Fig. 4b). With the first laser also on and generating a 13 keV modulation, the longitudinal phase spaces corresponding to the net acceleration and net deceleration cases are shown in Fig. 5c and Fig. 5d, respectively.

In Fig. 5c and Fig. 5d, it can be clearly seen that injection of optical micro-bunches allows many more particles to receive a similar energy shift, compared to those in a single stage IFEL. We also point out the 'W' and 'M' shapes that appear in the distributions in Fig. 5c and Fig. 5d. Analysis indicates that this structure is due to the nonlinear energy chirp in the beam longitudinal phase space (Fig. 5a). The energy chirp (correlation between energy and longitudinal position) of the beam together with the momentum compaction of chicane C2 shifts the laser modulation wavelength to $\lambda_1 = \lambda/C$, where C is the compression factor of the chicane [29]. Looking at Fig. 5d as an example, the wavelength shift results in a small phase shift (a few nm per laser cycle) between the two laser modulations, and after about 100 optical cycles the modulation accumulates a π phase shift that gives the optical micro-bunches around $z \approx \pm 80$ μm net acceleration (note the optical micro-bunches around $z = 0$ is net decelerated). When projected to the energy space, these net accelerated particles lead to the additional peak around $\Delta E = 180$ keV, as observed both in experiment and simulation (magenta dashed-dotted lines in Fig. 4). After accumulating another π phase shift, the optical micro-bunches around $z \approx \pm 120$ μm are net decelerated. Note, the quadratic energy chirp results in larger compression factors at larger z which speeds up the phase shift for particles farther away from the reference particle such that only 50 cycles are needed to accumulate the second π phase shift. This time-dependent phase shift gives the 'W' and 'M' shapes in the beam longitudinal phase spaces shown in Fig. 5c and Fig. 5d.

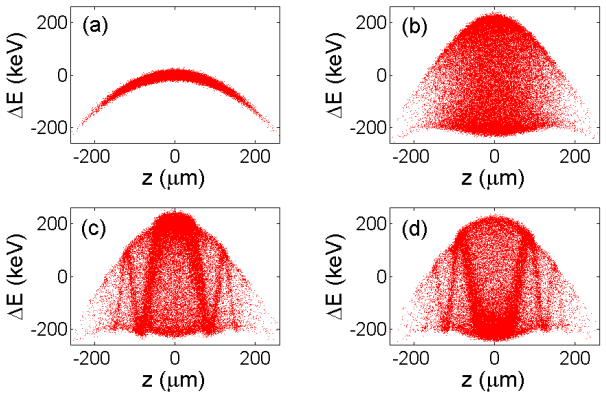

FIG. 5: Simulated beam longitudinal phase space at the entrance to (a) and exit of a cascaded IFEL [(b), (c) and (d)]: (b) with only the second laser on; (c) net acceleration with both lasers on; (d) net deceleration with both lasers on.

In summary, we have presented the first experimental demonstration of a cascaded IFEL at optical wavengths. We have shown that injection of precisely prepared optical micro-bunches allows net acceleration or deceleration of the beam in an IFEL, depending on the relative phase of the two laser modulations. While the net energy shift in our experiment is ~ 200 keV, much smaller than the beam energy (limited by the available laser energy in our experiment), it is an order of magnitude larger than the global beam energy spread, (and two orders of magnitude larger than the slice energy spread) and thus ideal for demonstrating both the fundamental physics and key advantages of cascaded optical IFELs. In this experiment, the beam is accelerated via the third harmonic interaction, which in principle allows one to lower the required beam energy for injection into an IFEL, promising further reductions in the size and cost of such advanced accelerators. The experimental results are in excellent agreement with simulations, particularly in the observed phase shift of the modulations from the nonlinear energy chirp. The demonstrated technique paves the way for generating high quality electron beams with narrow energy spread in direct laser accelerators (not limited to IFELs) driven by high-power optical lasers, and marks an important step towards more compact and affordable particle accelerators.

This work was supported by the US DOE Office of Basic Energy Sciences using the NLCTA facility which is partly supported by the US DOE Office of High Energy Physics under Contract No. DE-AC02-76SF00515.

*dxiang@slac.stanford.edu

†Currently a visiting student at SLAC

[1] L. Evans and P. Bryant, Journal of Instrumentation, 3, S08001 (2008).
[2] P. Emma *et al.*, Nature Photon. 4, 641 (2010).
[3] T. Tajima and J.M. Dawson, Phys. Rev. Lett. 43, 267 (1979).
[4] W. Leemans *et al.*, Nat. Phys. 2, 696 (2006).
[5] J. Liu *et al.*, Phys. Rev. Lett. 107, 035001 (2011).
[6] R. Palmer, J. Appl. Phys. 43, 3014 (1972).
[7] E. Courant, C. Pellegrini, and W. Zakowicz, Phys. Rev. A 32, 2813 (1985).
[8] W. Kimura *et al.*, Phys. Rev. Lett. 86, 4041 (2001).
[9] W. Kimura *et al.*, Phys. Rev. Lett. 92, 054801 (2004).
[10] P. Musumeci *et al.*, Phys. Rev. Lett. 94, 154801 (2005).
[11] E. Esarey, C. Schroeder, and W. Leemans, Rev. Mod. Phys. 81, 1229 (2009).
[12] ATLAS Collaboration, Phys. Lett. B 716, 1 (2012).
[13] CMS Collaboration, Phys. Lett. B 716, 30 (2012).
[14] A. Tremaine *et al.*, Proc. of PAC11, p1, New York, 2011.
[15] S. Anderson *et al.*, Proc. of IPAC12, p2795, New Orleans, 2012.
[16] J. Moody, *et al.*, AIP Conf. Proc. 1507, 482 (2012).
[17] J.P. Duris, P. Musumeci, and R.K. Li, Phys. Rev. ST Accel. Beams 15, 061301 (2012).
[18] L.-H. Yu, Phys. Rev. A 44, 5178 (1991).
[19] S. Pottorf and X. J. Wang, in 18th Advanced ICFA Beam Dynamics Workshop on Quantum Aspects of Beam Physics, edited by P. Chen (World Scientific Publishing Co., Singapore, 2002), p. 232.
[20] G. Stupakov and M. Zolotorev, in Proceedings of FEL 2011, Shanghai, China (2011), pp. 4548.
[21] D. Ratner and A. Chao, in Proceedings of FEL 2011 Conference, Shanghai, China (2011), pp. 5356.
[22] E. Hemsing and D. Xiang, Phys. Rev. ST Accel. Beams 16, 010706 (2013).
[23] C. Sears *et al.*, Phys. Rev. ST Accel. Beams 11, 101301 (2008).
[24] D. Xiang *et al.*, Phys. Rev. Lett. 105, 114801 (2010).
[25] D. Xiang *et al.*, Phys. Rev. Lett. 108, 024802 (2012).
[26] X.J. Wang, X. Qiu and I. Ben-Zvi, Phys. Rev. E 54, R3121 (1996).
[27] Z. Huang *et al.*, Phys. Rev. ST Accel. Beams 13, 020703 (2010).
[28] P. Musumeci, C. Pellegrini, and J. Rosenzweig, Phys. Rev. E 72, 016501 (2005).
[29] T. Shaftan and L.-H. Yu, Phys. Rev. E 71, 046501 (2005).